MATERIALS SCIENCE

Metal-metal interactions in correlated single-atom catalysts

Jieqiong Shan[1], Chao Ye[1], Yunling Jiang[1], Mietek Jaroniec[2], Yao Zheng[1]*, Shi-Zhang Qiao[1]*

Single-atom catalysts (SACs) include a promising family of electrocatalysts with unique geometric structures. Beyond conventional ones with fully isolated metal sites, an emerging class of catalysts with the adjacent metal single atoms exhibiting intersite metal-metal interactions appear in recent years and can be denoted as correlated SACs (C-SACs). This type of catalysts provides more opportunities to achieve substantial structural modification and performance enhancement toward a wider range of electrocatalytic applications. On the basis of a clear identification of metal-metal interactions, this review critically examines the recent research progress in C-SACs. It shows that the control of metal-metal interactions enables regulation of atomic structure, local coordination, and electronic properties of metal single atoms, which facilitate the modulation of electrocatalytic behavior of C-SACs. Last, we outline directions for future work in the design and development of C-SACs, which is indispensable for creating high-performing new SAC architectures.

INTRODUCTION

An ideal catalyst features maximum exposed active sites and optimal intrinsic activity per site to facilitate heterogenous reactions occurring on the solid surface (*1*–*4*). An increase in the amount of exposed active sites can be achieved by decreasing the size and improving the dispersion of active species (*3*, *5*). Inspired by molecular homogenous catalysts that exhibit 100% atomic utilization of metal sites, the fabrication of heterogenous catalysts with atomically dispersed metal atoms on various substrates has been achieved. Since the concept of single-atom catalysts (SACs) was first established in 2011 (*6*), most transition metals and noble metals have been extensively explored as metal single atoms on various types of substrates including carbons (*7*, *8*), metal oxides (*9*–*11*), metal sulfides (*12*), etc. The positive charge of the supported metal atoms originates from the bonds formed between the metal and substrate, leading to the electron transfer from the central metal sites to the substrate (*13*). This type of metal-support interactions has been extensively investigated in SACs to regulate the electronic structure of catalysts, which consequently affects the intrinsic activity of active sites toward various electrocatalytic reactions (*14*–*17*).

Although substantial compositional diversity has been achieved in SACs, metal single atoms are generally dispersed randomly and uncontrollably on substrates, leading to a lack of electronic synergy among metal active sites (*18*, *19*). Recently, an emerging class of catalysts with adjacent metal single atoms exhibiting atomic-scale site-to-site interaction has been reported with unique geometric features and enhanced electrocatalytic performance (*20*–*22*). Considering the spatial correlation among metal single-atom sites, this type of catalysts can be denoted as correlated SACs (C-SACs). Compared with the conventional SACs with fully isolated single-atom sites that exhibit solely MS interactions, an additional type of interactions in C-SACs, namely, metal-metal interactions, can induce evident electronic effects via electron transfer between adjacent metal single atoms (*14*, *23*, *24*). Since the number and type of the neighboring atoms in the first and second coordination shells significantly influence the local geometry and charge density of metal centers (*25*), the C-SACs with additional central metal atoms can potentially exhibit great structural flexibility (Fig. 1). Compared with isolated single atoms in conventional SACs, the correlated metal atoms in C-SACs may provide flexible adsorption configuration for reaction intermediates and produce intersite synergistic effect due to the interplay of metal-metal and metal-support interactions. In addition, unlike the supported metallic clusters/nanoparticles that adopt close-packing geometric modes with fixed structures, the correlated metal single atoms can exhibit a variety of geometric structures, demonstrating much higher flexibility in tuning electronic and electrocatalytic properties of C-SACs. For example, the short-range ordered Ir single atoms integrated in the Co oxide spinel lattice exhibit Ir-Ir interaction, which facilitates the modulation of electronic states of actives sites and results in exceptional electrocatalytic activity in acidic oxygen evolution reaction (OER) (*26*). In addition, diatomic metal pairs [e.g., Zn-Co (*27*), Ni-Fe (*28*), Pt-Ru (*29*), etc.] coordinated on carbon-based supports have been suggested to have favorable electronic properties toward various electrocatalytic applications. Although both interactions play important roles in C-SACs, as metal-support interactions have been critically assessed in a few reports (*30*, *31*), the current review is focused on the evaluation of metal-metal interactions in C-SACs.

Metal-metal interactions originate from the electronic perturbations among correlated metal single atoms and generally involve d orbital hybridization of transition/noble metal sites. Because of the wide availability and high variability of d orbitals, the metal-metal interactions create enormous opportunities for structural regulation in C-SACs (*32*). Apart from the direct influence from neighboring metal sites, the metal-metal interactions between correlated metal single atoms are significantly affected by the type of substrate in regard to the charge density, local coordination, and topological structures of metal centers. To investigate the metal-metal interactions between metal single atoms and thus understand the unique geometric and electronic structures of C-SACs, various techniques including advanced electron microscopy (*33*, *34*), theoretical computations (*35*), and ex situ and in situ spectroscopic characterizations

[1]School of Chemical Engineering and Advanced Materials, The University of Adelaide, Adelaide, SA 5005, Australia. [2]Department of Chemistry and Biochemistry and Advanced Materials and Liquid Crystal Institute, Kent State University, Kent, OH 44242, USA.
*Corresponding author. Email: yao.zheng01@adelaide.edu.au (Y.Z.); s.qiao@adelaide.edu.au (S.-Z.Q.)

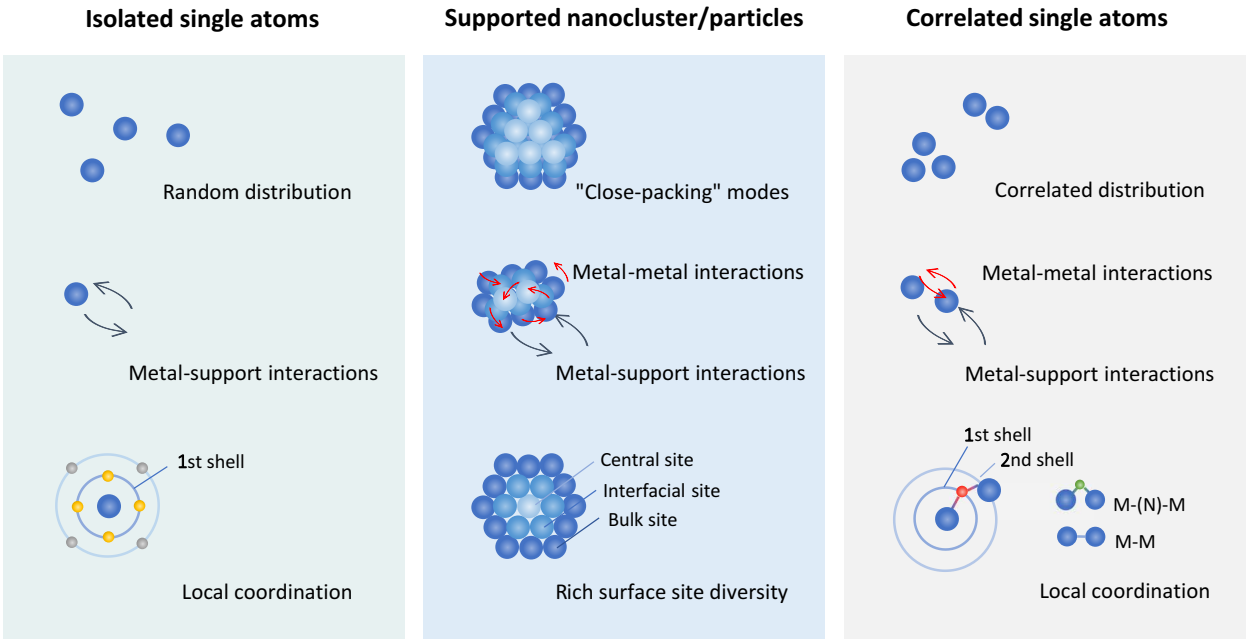

Fig. 1. C-SACs with metal-metal interactions. Comparison of C-SACs with the conventional isolated SACs and supported metallic cluster/nanoparticle catalysts from the perspective of spatial distribution, intersite interactions, and local coordination.

(*36*) have been applied to create fundamental knowledge at the atomic level. It is worth mentioning that in the supported metal nanoclusters, although intersite metal-metal interactions can be observed, the rich diversity of metal atoms in geometric and electronic structures makes the studies of these interactions difficult (*37*, *38*). In addition, considering the lack of lattice confinement of the metal atoms, the supported nanoclusters are not considered as "single-atom" materials; thus, they are not discussed in this review.

So far, the emerging class of C-SACs shows promising prospects for various electrocatalytic reactions because of the unique structural characteristics and higher flexibility in regulating their electrocatalytic behavior as compared to conventional SACs. The high potential of C-SACs to exhibit remarkable performance in a wide range of heterogenous catalytic applications calls for a critical assessment of the current research advances in this field. The aim of this review is to provide a rational overview of C-SACs and to achieve a critical understanding of the geometric structure-catalytic property relationship affected by metal-metal interactions. First, a broad picture of this class of catalysts is presented by discussing the structural features, structural influence of substrate, and the presence of metal-metal interactions in C-SACs. In addition, the unique atomic structure, local coordination, and electronic structure of C-SACs is assessed in comparison to the conventional isolated SACs. Last, future research directions are outlined to guide the rational design and deepen the fundamental understanding of C-SACs.

STRUCTURAL FEATURES OF CORRELATED SINGLE ATOMS

The high variability of d orbitals and spatial geometries in transition metals permits the regulation of the correlated metal sites. Specifically, the electronic structures of C-SACs with metal-metal interactions can be regulated by adjusting bonding polarity, bonding coordination, atomic arrangement, and topological structures.

Homo/heteronuclear metal sites

Considering homo- and heteronuclear metal sites, the metal-metal bonds in C-SACs can be classified as nonpolar bonds and polar bonds, respectively (Fig. 2A). Unlike the isolated single metal atoms in conventional SACs, the homo/heteronuclear metal sites are both capable to provide multiple reaction adsorption sites but exhibit different local charge distribution (*39*). Compared with homonuclear SACs with identical central metal atoms and symmetric charge distribution, the heteronuclear SACs involving different metal single atoms (e.g., Co/Zn, Fe/Co, Fe/Ni, etc.) may potentially exhibit structural deformation and asymmetric charge density. The metal-metal bonding between heteronuclear metal sites may cause a substantial perturbation in electronic structure (*40*, *41*). In principle, the pairing and coupling of different single-atom sites would induce charge polarization and increase the electronic states toward the Fermi level (*24*). For example, the interaction between Pd and Co in a PdCo single-atom-layer alloy leads to the splitting of the unoccupied 4d band indicating strong coordination between Pd and Co (*42*). This two-dimensional oriented coordination causes the valence/empty d- and p-bands to split into a lower-energy band in the *x-y* plane, which is conducive to in-plane stability, and a higher-energy band in the *z* direction, which is beneficial for reactivity along this direction. In certain complicated reactions involving multistep proton-electron transfer, e.g., carbon dioxide reduction reaction (CO_2RR), the homo- and heteronuclear metal sites may offer different absorption configurations for various intermediates and induce different reaction mechanisms. For example, a Ni/Cu-N-C catalyst with synergistic NiN_4 and CuN_4 moieties showed an outstanding catalytic activity and selectivity toward CO_2RR, achieving a maximum carbon monoxide (CO) Faraday efficiency of 99.2% (*43*). The heteronuclear monomers exhibit charge redistribution on Ni centers induced by neighboring CuN_4 sites, which results in enhancing adsorption of *COOH and facilitating CO generation. A recent report also highlights

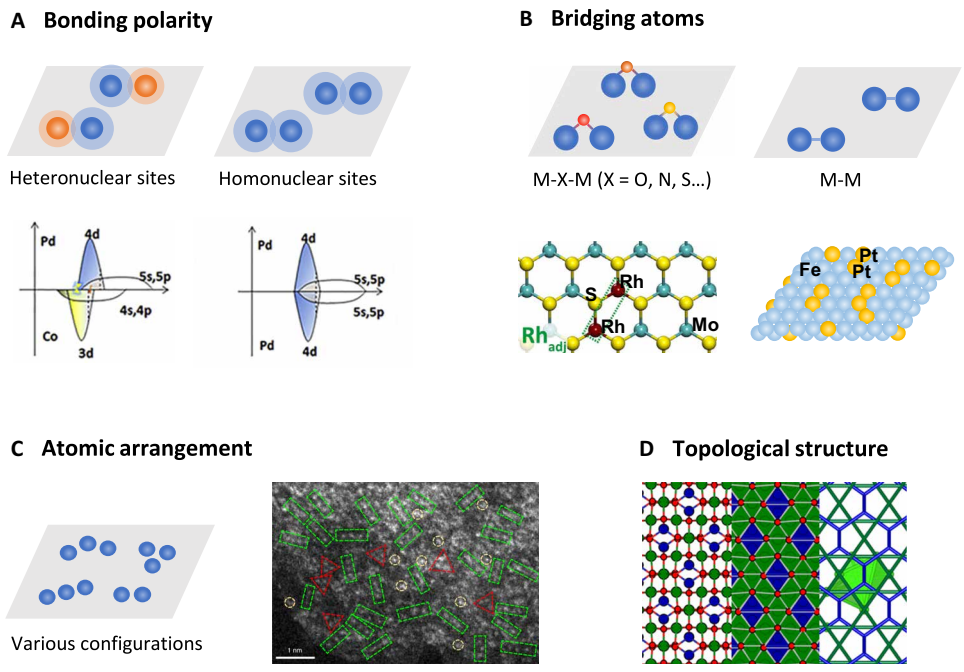

Fig. 2. Structural features involved in the metal-metal interactions of C-SACs. (**A**) Bonding polarity of metal-metal interactions, reproduced with permission from Elsevier (*42*). (**B**) Bridging atoms between metal sites, reproduced with permissions from John Wiley and Sons (*49*). (**C**) Atomic arrangement of metal single atoms, reproduced with permission from the Nature Publishing Group (*55*). (**D**) Schematic illustration of topological structure of metal single atoms in Co_3O_4 matrix. From left to right: the crystal structure along <110> projection, corresponding projected tiling of Co_3O_4 (green, blue, and red refer to Co_{oct}, Co_{tet}, and oxygen), and topology illustration of **crs** (green) and **dia** (blue) nets with a polyhedron of metal single-atom sites (light green).

that a homonuclear Cu-Cu atomic catalyst enables efficient CO electroreduction to C^{2+} products (*44*). As demonstrated by theoretical calculations, the electroreduction of two CO molecules and subsequent carbon-carbon coupling to ethylene and acetate are boosted by dual Cu atomic sites, while if one of the dual Cu atoms is substituted by Ni atom, the CO adsorption is excessively strong to suppress the C^1 reduction pathway. However, for homo/heteronuclear metal sites consisting of two transition metal atoms that both exhibit strong CO adsorption, it is more likely that CO_2RR follows the C^1 reduction pathway, which has been demonstrated by recent studies for Fe-Fe homonuclear sites (*45*) and Fe-Ni heteronuclear sites (*23*, *28*).

Bridging atoms

Depending on the type of substrate, synthesis conditions, and chemical nature of the involving atoms, the single metal atoms exhibit different local coordination configurations (*25*, *46*, *47*). The correlated metal single atoms are either bonded with each other in the first coordination shell or being connected via a nonmetal atom linker, thus exhibiting significantly increased complexity in local coordination. Anchored on different substrates, such as metals, metal (hydro)oxides, metal sulfides, metal phosphides, (pristine or doped) carbons, etc., the correlated metal single atoms exhibit various coordination configurations including M-O-M (*48*), M-N-M (*43*), M-S-M (*49*), and direct M-M bonding (Fig. 2B) (*50*). Depending on the bridging atoms, the coordination configuration may result in redistributed electron density on the metal centers and consequently lead to regulated reaction mechanism (*51*, *52*). For example, in a Pt-O-Pt/CeO_2 catalyst, the correlated Pt atoms adopt an oxo Pt-O-Pt configuration, which is distinct from the Pt-Pt coordination in the close-packing Pt nanoparticles and clusters (*53*). The Pt atoms of Pt-O-Pt/CeO_2 are only bridged by oxygen in its first coordination shell, resulting in a somewhat similar behavior of these Pt atoms to the isolated Pt_1 atoms in terms of the Pt-O local structures. Apart from maximum atomic utilization like isolated Pt single atoms, the oxygen bridging sites facilitate a so-called "oxygen migration" mechanism on Pt centers to effectively activate and use oxygen intermediates toward low-temperature CO oxidation. Therefore, it is expected that the bridging sites either can potentially participate in the catalytic reactions directly as active sites or affect adsorption of reaction intermediates. In addition, it has been demonstrated in conventional SACs that the nonmetal coordination atoms with different radius and electronegativity can induce asymmetric charge distribution on metal centers (*54*), suggesting that the bridging atoms (e.g., O, N, and S) between correlated single atoms can be engineered to regulate catalytic properties of C-SACs. It needs to be clarified that most of the current reported correlated single atoms are coordinated with nonmetal bridging sites, yet for the convenience and simplicity of discussion, the metal coordination will be denoted as M-M without specifically noting the bridging site in the following sections.

Atomic arrangement

When correlated metal single atoms are immobilized on substrates, the spatial arrangement of the metal atoms and the involving lattice atoms can be regulated to exhibit various local coordination configurations with different metal-metal interactions. For example, in a Ni_1Cu_2/g-C_3N_4 catalyst, the statistical analysis based on the aberration-corrected high-angle annular dark-field scanning transmission electron microscopy (HAADF-STEM) images suggest that the Ni_1Cu_2 metal centers exist dominantly as linear trimers and partially as triangular trimers (Fig. 2C) (*55*). This can be attributed to the synthetic strategy

in which Ni atoms tend to bridge the predeposited single Cu atoms to form new linear Cu-Ni-Cu trimers. In addition, integrated measurements have demonstrated that the exceptional catalytic activity of Ni_1Cu_2/g-C_3N_4 catalyst come solely from the prevailing linear trimers as dictated by the Cu-Ni metal-metal interactions. This demonstrates the close relation between atomic arrangement and catalytic properties on correlated metal centers.

Topological structures

Different from isolated single atoms exhibiting random atomic distribution, the spatially correlated single atoms within sublattice of substrates can possibly exhibit identical topological structures with those of substrates. Thus, it is a promising strategy to achieve artificially designed topological structures of metals by incorporating correlated metal single atoms in substrates with specific underlying topologies. Taking Co_3O_4 as an example, the octahedral Co (Co_{oct}) and tetrahedral Co (Co_{tet}) sublattices adopt **crs** (cristobalite) and **dia** (diamond) topologies, respectively. When Co_{oct} sites are selectively substituted in the Co_3O_4 framework, the correlated metal single atoms can exhibit identical **crs** topology with the host sublattice (Fig. 2D). The diversification of topological structures provides much more space in fine-tuning metal-metal and metal-support interactions in catalyst systems by regulating atomic distance, local coordination, and electronic structure of the metal centers, all of which contribute to the modulation of catalytic performance of C-SACs. Correlated metal single atoms incorporated in substrates can exhibit a series of identical topological structures with those of substrates such as **crs**, **dia**, **fcu** (face-centered cubic), **hex** (hexagonal), **pcu** (primitive cubic), **bcu** (body-centered cubic), etc. This strategy may eliminate the close-packing limitation of metallic phases and greatly diversifies the topological structures of metals, leading to a new catalyst family that is distinct from conventional SACs and nanocluster/particles.

STRUCTURAL INFLUENCE OF SUBSTRATE

Compared with isolated SACs with simple local coordination, C-SACs exhibit higher flexibility in geometric, electronic, and topological structures by manipulating metal-metal interactions, all of which are largely dictated by the type of substrate. The commonly adopted substrates fall into two categories: carbon-based substrates and metal compound substrates.

Carbon-based substrates

The incorporation of various heteroatoms in the local coordination of metal single atoms can induce different electronic structure via charge transfer between metal center and the lattice nonmetal atoms. As the prime example of carbon-based material, the nitrogen-doped carbon has been extensively adopted as a substrate, resulting in typical M-N-C structure with supported metal single atoms generally consisting of M-N_x moieties (*56*–*58*). In M-N-C system with correlated metal single atoms, plentiful structural defects induced by nitrogen doping can act as anchoring sites for single atoms; meanwhile, the porous structures of carbonaceous materials can be modulated by nitrogen doping to construct confined space for metal single atoms. Besides, the nitrogen dopants can effectively modulate the intrinsic electronic structures of adjacent atoms to facilitate adsorption of reaction intermediates (*59*). Depending on the varying geometric structure and composition of substrates, the local environment of metal sites, including coordination number and chemical bond, can be diversified (Fig. 3A) (*24*, *60*–*65*). Apart from nitrogen-doped carbon materials, some other coordination atoms such as O, S, and P have also been investigated as heteroatom dopants in the carbon matrix. However, a major limitation of carbon-based substrates is that the anchor sites of metal single atoms are nonuniform and highly dependent on the synthetic strategy (*66*, *67*), making difficult an effective regulation of the electronic and topological structures of metal sites.

Metal compound substrates

The metal compound substrates constitute of various classes of materials including transition metals (*68*, *69*), transition metal oxides (*70*, *71*), carbides (*72*), phosphides (*73*), dichalcogenides (*49*), etc. These metal compound substrates create a complex and flexible environment for the supported metal single atoms with various

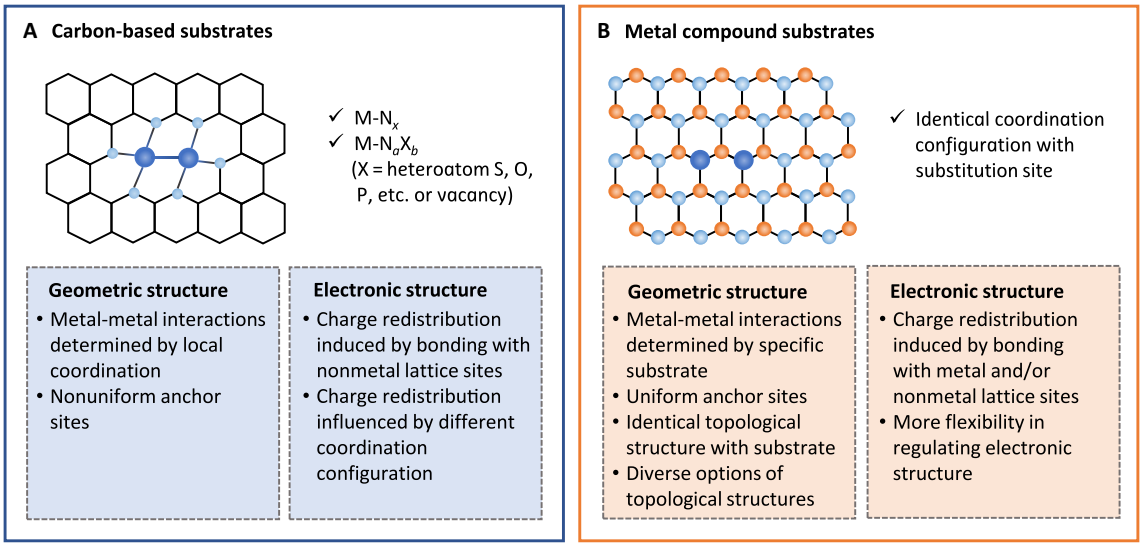

Fig. 3. The structural influence of substrates in C-SACs. The carbon-based (**A**) and metal compound (**B**) substrates are compared in terms of the geometric and electronic structures.

nonmetal and metal lattice atoms to bond with (Fig. 3B). In addition, because of the relatively high atomic number, the metal compound substrates always have more complex electronic structure than the carbon-based counterparts, which indicates that there is more space for regulation of electronic structure in metal-metal interactions. More importantly, most of the metal compound substrates have ordered and crystalline structures, providing uniform sites for correlated metal single atoms to anchor on. For example, in the case of metal oxide as supports, single atoms are commonly hosted by cationic vacancies due to the facile oxidation of noble metal atoms by the uncapped oxygen atoms (*30*). Such specified atomic arrangement permits the correlated single atoms to adopt diverse topological structures of the substrates.

Adoption of metal compound substrates may achieve another benefit that sometimes they can be activated toward electrocatalytic reactions upon incorporation of single atoms. For example, the iridium dopants in strontium titanates (STO) have been demonstrated to activate the intrinsically inert titanium sites by optimizing their electronic structure and strengthening oxygen adsorption on them (*74*), leading to about 10 times higher catalytic activity than that of the benchmark IrO_2 catalyst for OER in acidic environment. In addition, the metal compound substrates can participate in the electrocatalytic reactions via synergistic effect between single atoms and substrate sites. For example, we demonstrated that the correlated Ir single atoms within the lattice of Co_3O_4 can construct a synergistic active site of nanodomain with Ir sites and enclosed Co sites (*26*). Similarly, the correlated Pt single atoms in Pt/MoS_2 catalyst were suggested to form active center with the corresponding activated S atoms, which act as sites for the dissociation of H_2 and adsorption of intermediates during the CO_2 hydrogenation (*22*).

CREATING METAL-METAL INTERACTIONS IN C-SAC

Creating environment for metal-metal interactions in SACs requires a careful design and modulation of local arrangement of single metal atoms confined in the lattice of substrates. To achieve this, a few strategies have been reported to incorporate additional metal sites in the proximity of the central metal single atoms.

Regulating site density of single atoms

The intersite distance between atomically dispersed metal moieties has been proposed as a descriptor to quantitatively evaluate the electronic structure of C-SACs. A very straightforward strategy to regulate the metal-metal interactions in C-SACs is to tune the site-to-site distance by altering the site density in the lattice of substrates (Fig. 4A) (*71*). Achieving highly loaded and stable single atoms is challenging because of the high mobility of atomically dispersed metal species during synthesis (*5*). In the conventional SACs, the low loading of metal atoms results in configurations with single sites far apart from each other and lack of distance synergy. The

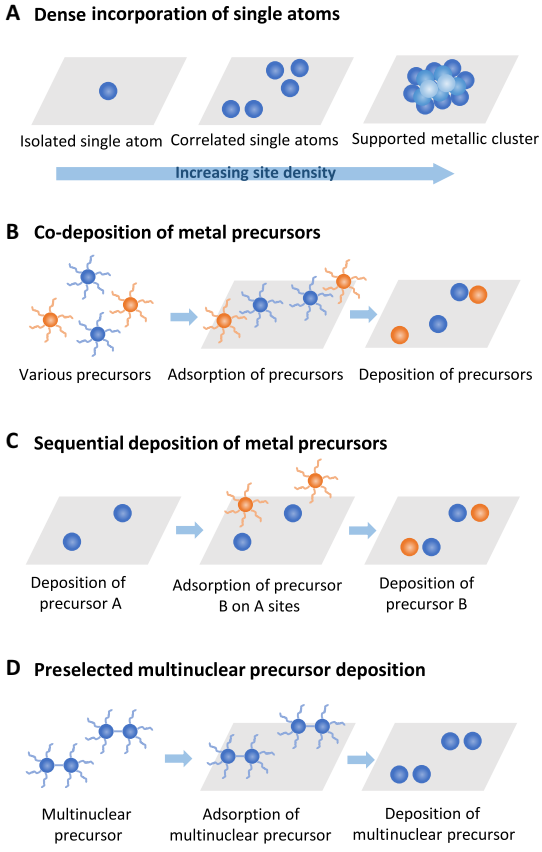

Pros:
- Tunable correlation degree of metal sites
- Wide applicability to various metal single atoms and substrates
- Easy implementation and low cost

Cons:
- Difficulty in preparing heteronuclear sites
- Difficulty in controlling coordination configuration and distribution uniformity

Pros:
- Applicability to prepare heteronuclear sites
- Easy implementation and low cost

Cons:
- Difficulty in controlling coordination configuration and distribution uniformity
- Weak metal-metal interactions due to random atomic distance of metal atoms

Pros:
- Well-controlled local coordination and uniform distribution
- Applicability to prepare heteronuclear sites

Cons:
- Limited range of available metal precursors and substrates
- Complicated implementation and high cost

Pros:
- Applicability to prepare metal sites with desired size
- Well-controlled local coordination and uniform distribution

Cons:
- Difficulty in preparing heteronuclear sites
- Limited range of available metal precursors

Fig. 4. The formation of C-SACs with metal-metal interactions. Illustration of strategies including (**A**) dense incorporation of single atoms, (**B**) co-deposition of metal precursors, (**C**) sequential deposition of metal precursors, and (**D**) deposition of preselected multinuclear metal precursors. The pros and cons are summarized in the right column.

increased site density of single atoms makes possible the formation of unique local configuration with tunable intersite distance and metal-metal interactions. For example, the fabrication of neighboring Pd single atoms with synergetic interactions by increasing the Pd loading up to 5.6% in the lattice of SiC has been recently demonstrated (*20*). The neighboring Pd atoms exhibited cooperative interactions to lower the energy of key reaction steps, resulting in greatly improved catalytic performance in comparison with that for the isolated Pd single-atom counterparts. A key factor in this strategy is to limit the concentration of single metal atoms that can be incorporated in the specific substrate lattice. The concentration much below the limit leads to fully isolated metal sites, while that exceeding the limit leads to the formation of metallic nanoclusters or nanoparticles outside the substrate lattice. We recently reported an "ion-exchange-pyrolysis" strategy to integrate short-range ordered Ir single atoms in the octahedral Co site of Co oxide spinel lattice (*26*). The obtained $Ir_nCo_{3-n}O_4$ hybrid materials featured the presence of both metal-support and metal-metal interactions, making further modulation of the electronic structure of active sites possible as contrasted to the isolated SAC counterpart.

The construction of densely populated single metal sites is often adapted from the methodology used in the synthesis of conventional SACs and is often combined with wet chemistry approach. Therefore, it represents a desirable and general strategy for investigation of metal-metal interactions because of its simplicity and wide applicability. However, major technical issues lie in the difficulty in precisely controlling the local coordination and construction of heteronuclear intersite interactions. In addition, the choice of substrate and the corresponding concentration limit of metal single atoms incorporated in the specific substrate need to be carefully explored.

Co-deposition of various precursors

To investigate the metal-metal interactions in heteronuclear metal pairs, the co-deposition of two or more types of metal ion precursors is often adopted (*75*). Generally, the well-mixed various precursors are first adsorbed on the surface of substrate; then, a deposition process (e.g., pyrolysis and chemical vapor deposition) is applied to fix the metal species in the lattice of substrate (Fig. 4B). If necessary, a following-up acid treatment process can be adopted to remove the metal particles. For example, a NiFe-diatomic site catalyst was synthesized by pyrolyzing mixture of carbonaceous precursor together with iron and nickel precursors in argon atmosphere, followed by washing with 2 M HCl solution to remove iron and nickel particles (*28*). Ni and Fe single atoms in the resultant material are suggested to form atomic pairs on the N-doped graphene substrate due to metal-metal interactions. Nevertheless, one challenge in this synthesis strategy is that the various metal species usually disperse in the substrates randomly, leading to simultaneous formation of homonuclear and heteronuclear metal sites. A solution to this issue is the use of self-assembly chemistry to form coordination between heteronuclear metal species by careful selection of metal precursors. Yang and co-workers (*76*) reported the synthesis of W-Mo atomic pairs anchored in the N-doped graphene substrate by adopting polyoxometalates (POMs) as metal sources in a hydrothermal process in graphene oxide solution and followed by chemical vapor deposition process. The tungstic acid and molybdate precursors were transformed into Mo aquo ligands $[MoO_4(H_2O)_2]^{2-}$ and hydrogentungstate anion $[WO_3(OH)]^-$ species during the hydrothermal process and then underwent self-assembly via dehydration condensation reaction. This allows a more precise control of the formation of W-Mo heteronuclear atomic pairs with metal-metal interactions. This study presents an alternative way to develop locally coordinated heteronuclear metal atoms with metal-metal interactions by adopting POMs as metal precursors. As the deposition of metal atoms is often achieved via a pyrolysis process under high temperature, elements with relatively lower vaporization temperature, e.g., zinc, can be adopted to provide a second metal source. For example, the fabrication of Pd-Zn dual sites has been realized by a Zn vapor-assisted strategy (*77*). First, the prepared ZnO nanorods were adopted as a substrate for a polydopamine coating to load Pd ion precursors. Then, during high-temperature reduction process in H_2 atmosphere, the polydopamine layer transforms into N-doped carbon to restrict the migration of Pd atoms, and the Zn vapor is generated from ZnO for bonding Pd atoms to form Pd-Zn dual sites.

The co-deposition strategy can be easily implemented to fabricate heteronuclear sites with low cost, while it is challenging to regulate local coordination and distribution of various metal species that have tendency to disperse randomly on the substrates. In addition, the resultant metal-metal interaction can be weak and uncontrollable because of random atomic distance among metal single atoms.

Sequential deposition of precursors

As a powerful tool to achieve the bottom-up construction of catalytic materials evenly and accurately on a high-surface area substrate, atomic layer deposition (ALD) functions through two sequential self-limiting surface reactions separated by inert gas purging (Fig. 4C) (*78*). It was demonstrated that Pt_2 dimer can be sequentially deposited on a graphene support in a sequential manner using Pt ALD (*79*). The first cycle of Pt ALD assures Pt nucleation on graphene defect sites to form anchored Pt_1 single atoms. In the following cycle, the Pt_1 sites serve as the new nucleation sites for anchoring only one Pt precursor molecule due to the steric hindrance effect, which is known as a self-limiting growth approach. Carefully controlled deposition conditions were then adopted to form Pt_2 metal sites by removing the ligand without causing metal aggregation. In addition to homonuclear correlated metal sites, ALD can also be applied to fabricate heteronuclear sites by adopting different metal precursors in the cycles. For example, Pt-Ru dimers on N-doped carbon nanotube were achieved by using Ru precursor in the second cycle to anchor Ru atoms on the Pt_1 sites (*63*). A major challenge of the ALD strategy is the high-cost, complicated implementation and limited choice of metal precursors and substrates.

Although coordinated in substrate lattice, the single metal atoms might undergo reconstruction under reaction conditions, which, in turn, offers an opportunity to design desired local metal configurations. Bai and co-workers (*80*) reported the in situ formation of Co-Fe dual-atom catalyst starting from a single-atom Co precatalyst in OER electrocatalysis. Operando spectroscopic observations illustrate the activation process of Co-N-C structure that promotes incorporation of Fe ions from the electrolyte. Under positive potential of OER process, the $[Fe(OH)_4]^-$ species in the electrolyte can be adsorbed onto the electrode, where the Co single atoms are the preferred sites, leading to the formation of dimetric Co-Fe units with heteronuclear metal-metal interactions. Further investigation extended this in situ electrochemical transformation strategy to synthesize Co-, Fe- and Ni-containing double-atom catalysts from their single-atom precursors (*81*).

Preselected precursor deposition

One strategy to achieve precise control of atomic metal sites with defined local coordination configurations is to adopt preselected precursors with multinuclear metal species as metal sources (Fig. 4D). For example, by using palladium salts with different sizes of metal species including $Pd(NH_3)_4(NO_3)_2$, $[PdCl(C_3H_5)]_2$ (allyl palladium chloride dimer), and $[Pd(OAc)_2]_3$ (palladium acetate trimer) as metal precursors, a series of low-nuclearity Pd catalysts were obtained by microwave-assisted deposition of the corresponding precursors onto exfoliated carbon nitride (ECN) substrate (*82*). The obtained Pd_1/ECN, Pd_2/ECN, and Pd_3/ECN catalysts exhibited different nearest neighbor distances between Pd atoms, allowing for the regulation of metal-metal interactions. Very recently, Ding and co-workers (*60*) reported the preparation of ligand-protected dinuclear $Ni_2(dppm)_2Cl_3$ cluster as metal precursor for the formation of Ni_2-N-C catalyst. The cluster was impregnated in a zeolite imidazolate framework 8–derived porous carbon and contributed to the formation of uniform atomically precise Ni_2 site in N-doped carbon. The Ni_2-N_6-C structure exhibits enhanced Ni-Ni interaction, which is absent in the conventional Ni_1-N_4-C structure synthesized by using a single-nuclear $Ni(dppp)_2$ precursor. In addition, deposition of mass-selected gas phase metal clusters combined with soft landing on supports is an efficient technique to precisely control size and local coordination environment of interacting metal sites (*83*). Although this strategy is mainly adopted to fabricate supported metal nanoclusters with defined size, it can also be adopted to achieve lattice confined single metal atoms by careful coordination with the substrate. Nevertheless, this strategy is only available for the formation of a limited range of homonuclear metal sites, and its implementation is complicated.

ATOMIC STRUCTURE ELUCIDATION

The prerequisite for investigating the metal-metal interactions in SACs is the identification of atomic structure and elucidation of local coordination environment of the single-atom metal sites. Although new characterization techniques exclusively available for C-SACs are currently limited, some unique capabilities of the classical techniques applied in the examination of conventional SACs can be used to obtain valuable information about atomic structure and local coordination of C-SACs. Because of the lack of long-range order of the metal sites, it is generally difficult to characterize single metal atoms by techniques focusing on crystalline structure, e.g., x-ray diffraction. The advances in electron microscopic characterization techniques provide strong support for direct observation and structural identification of the geometric features of this class of materials.

Atomic structure observations

Nowadays, the substantial development in microscopic technology makes the direct visualization of the atomic arrangements of metal single atoms possible by means of the aberration-corrected electron microscopy. Various techniques have been widely used for the identification of atomic structures including HAADF-STEM (*84*), single-atom electron energy loss spectroscopy (EELS) (*71*), line scan intensity profile (*85*), energy-dispersive x-ray spectroscopy elemental mapping (*86*), etc. An important basis of HAADF-STEM is that the imaging is based on Rutherford scattering in which image intensity for given atoms is roughly proportional to the square of the atomic number (Z^2) of the element (*87*). As a very suitable study object by HAADF-STEM, SACs contain at least two different elements, which are generally heavy metal atoms supported on lighter metal or nonmetal substrates, allowing bright contrast of the single metal atoms (*88*). Apart from direct visualization of single metal atoms based on atomic-resolution HAADF-STEM images, the corresponding techniques facilitate the elucidation of atomic structure and chemical properties of target metal atoms. Measured and analyzed by energy losses when an electron beam passes through the material, EELS helps one to determine the types and numbers of atoms, which makes it a good tool to investigate correlated homo- or heteronuclear single atoms. Similarly, line scan intensity profile can be used to illustrate atomic arrangement, average atomic distance, and relative height differences between adjacent atoms according to the different brightness of various atoms across the line (*89*).

Structural simulation

With the improvement of atomic resolution of HAADF-STEM technique, some practical procedures for image simulation provide strong support for a quantitative interpretation of the HAADF images, which facilitate identification of the local structure of metal sites. On the basis of the HAADF-STEM simulations of the proposed models involving the multislice method, a good agreement between simulations and experimental images can be adopted to determine the structure of materials (*90*). It is very straightforward to simulate two-dimensional materials. For example, in a two-dimensional hybrid consisting of Co arrays and MoS_2 nanosheets, the HAADF-STEM images and simulated patterns not only confirm the atomic dispersion of Co species but demonstrate the interface between 1T MoS_2 and 2H MoS_2 (*91*). Similarly, for Pt single atoms anchored in double transition metal MXene ($Mo_2TiC_2T_x$) nanosheets, the HAADF-STEM imaging and the corresponding simulation have been successful in demonstrating that these Pt atoms occupy Mo positions (*92*). In most common three-dimensional materials, however, such simulation is much more complicated. A plausible strategy is to conduct structural simulation from various projections and conceive the spatial structure of single metal atoms accordingly. We recently conducted structure simulation for Ir single-atom integrated Co oxide spinel based on HAADF-STEM images collected from various projections to achieve the explicit identification of the Ir sites (Fig. 5A) (*26*). A comprehensive simulation of the representative structural projections confirmed that Ir preferentially substitutes the cationic Co_{oct} sites in the Co_3O_4 structure. The doping configurations of Ir sites can be unambiguously determined, providing strong evidence regarding spatial structure of correlated Ir single atoms.

Statistical analysis

An important limitation factor for adopting microscopic techniques to study C-SACs is their ability to identify local structures instead of assessing the overall structure. In particular, the adoption of three-dimensional or noncrystalline substrates permits the display of correlated metal sites with multiple orientations, which makes the elucidation of the size and structure of metal sites difficult by simple visual observation. One strategy that has been used to deal with this issue is to perform statistical analysis of a large amount of metal atoms based on HAADF-STEM images collected at relatively larger scales. In the cases of C-SACs, the spatial distances between correlated metal atoms, e.g., W-Mo dual-atom pairs, can be measured and statistically compared to reveal the spatial structure (*76*, *82*, *93*). We also demonstrated the spatially correlated distribution of Ir

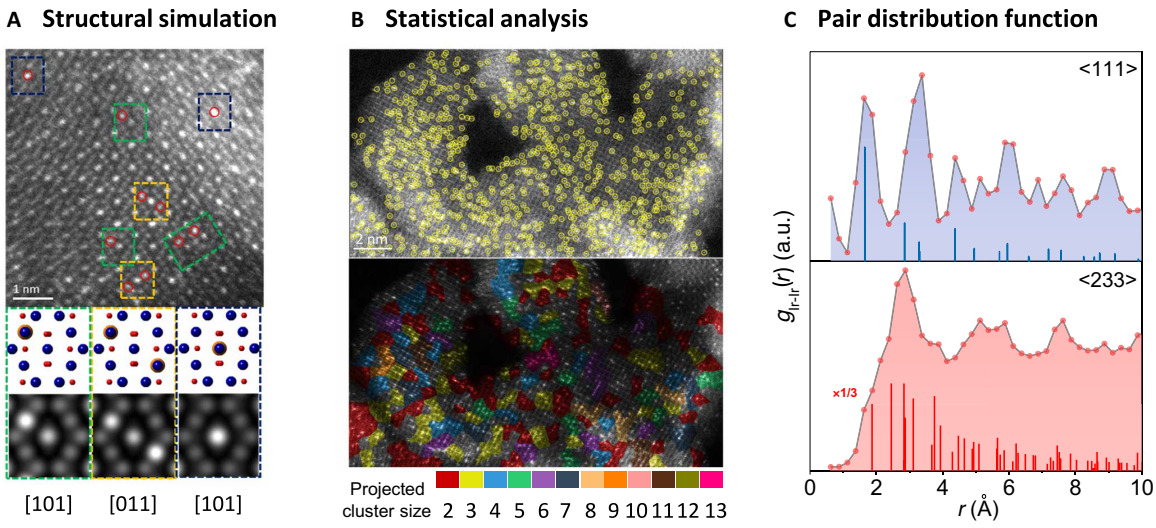

Fig. 5. The atomic structure elucidation of C-SACs with metal-metal interactions. (**A**) Structural simulation based on high-resolution STEM (HRSTEM) imaging and analysis. (**B**) Statistical analysis of a large number of metal single atoms to determine the spatial correlation. (**C**) Pair distribution function (PDF) curves obtained by HRSTEM analysis to elucidate spatial structure of metal single atoms. (A) to (C) are copied with permission from the American Chemical Society (*26*). a.u., arbitrary units.

single atoms in the Co oxide spinel framework based on the proper labeling and classification of these Ir sites (Fig. 5B) (*26*). Furthermore, the relative population of projected clusters with a certain size can be statistically analyzed and evaluated in terms of the mass fraction. Generally, it was found that most of the Ir sites adopt short-range order rather than exist as isolated sites within the cationic lattice of Co_3O_4; the mass fraction of clusters decreases with increasing cluster size.

Spatial structure analysis

The pair distribution function (PDF) analysis is a remarkable tool to elucidate the atomic arrangement in materials with high spatial resolution (*94*). To determine the spatial correlation of Ir sites in the lattice of Co_3O_4, we analyzed 4650 Ir sites in HAADF-STEM images along different projections to calculate the partial projected PDF (pPDF) (*26*). As shown in the pPDF profiles for <111> and <233> axes (Fig. 5C), multiple sharp correlation peaks unambiguously confirm that the majority of Ir sites show a short-range correlation. A comparison with the calculated pPDF histograms of the projected Co_{oct} cationic sublattice of Co_3O_4 along these projections confirms that these Ir sites adopt an identical spatial correlation with the Co_3O_4 host lattice. The presence of several correlation peaks below 4 Å for projected Ir-Ir pairs also indicates a high probability of local clustering of Ir sites within the spinel framework. Besides, PDF curves can also be obtained by high-energy x-ray scattering. For example, it was demonstrated that upon incorporation of Pt sites, the CeO_2 sample exhibits additional peaks corresponding to the correlated Pt_3O_4 structural fragments in the square planar environment on the (100) CeO_2 facet (*95*). This unique arrangement of Pt atoms and distorted CeO_2 surface were dictated by Pt-Ce metal-metal interactions and contributed to the effective redox properties of the hybrid materials.

LOCAL COORDINATION ANALYSIS

Beyond direct inspection of atomic structure, the investigation of local coordination environment of C-SACs can provide important evidence for metal-metal interactions between metal atoms. X-ray absorption spectroscopic measurements have been widely applied as a powerful tool to provide direct information on the local structure of target atoms. At the same time, Fourier transform infrared spectroscopy and temperature-programmed desorption spectroscopy (TPD) can be applied to provide indirect information about metal-metal interactions by monitoring chemisorption/desorption behavior of target atoms using various probe gas molecules. In addition, some surface-sensitive quantitative spectroscopic techniques, e.g., x-ray photoelectron spectroscopy (XPS), can be conducted to investigate the chemical state of correlated single atoms. The shift and proportion of deconvoluted XPS peaks can be applied to demonstrate the charge transfer and coordination between metal atoms (*50*).

X-ray absorption spectroscopy

The x-ray absorption near-edge structure (XANES) has been widely used to characterize average chemical state of target metal species by measuring the electron transition energy, which can be used to evaluate the interactions between single metal atoms and the neighboring atoms. Often coordinated with nonmetal atoms from the substrate, the metal single atoms generally exhibit near-edge between those of the corresponding metal foil and metal oxide references. Compared with isolated single atoms, the correlated metal sites tend to exhibit a slightly changed valence state due to the modified electron transition behavior affected by metal-metal interactions. For example, in a Ni/Fe-N-C catalysts with Ni-Fe dual-metal atom centers, the 3d and 4p orbital hybridization of the Ni central atoms can be displayed by the pre-edge peak. In contrast to Ni-N-C and Ni-Pc, the Ni/Fe-N-C exhibited an increased prepeak intensity, demonstrating that Ni species in Ni/Fe-N-C show the distortion of *D4h* symmetry due to the metal-metal coordination (*96*). Furthermore, the extended x-ray absorption fine structure (EXAFS) is often measured to qualitatively assess the local coordination environment of target atoms regarding bond distance and coordination number. In conventional SACs, the dominating first-shell coordination together with the absence of the second-shell metal-metal path in Fourier transformed (FT)–EXAFS spectra has been widely adopted

as one criterion to demonstrate the formation of isolated single atoms (*73*). In contrast, a weak first-shell coordination and strong second-shell coordination can be expected in EXAFS spectra of typical nanoparticles. Comparatively, in C-SACs, the simultaneous presence of metal-support and metal-metal interactions results in the positive signature of both coordination types. Fitting the experimental FT-EXAFS spectra can be used to provide information about local coordination including atomic distance and coordination number of metal-metal scattering path to evaluate the metal-metal interactions between correlated single atoms. In addition, on the basis of the possible structural models deduced by density function theory (DFT) calculations, the XANES spectra simulation based on the multiple scattering approach can be compared with experimental spectra to determine the distinct metal-metal coordination configuration of C-SACs in comparison with those in nanoparticles. For instance, the Fe K-edge FT-EXAFS spectrum of a Fe-Co dual-atom catalyst indicates a first-shell Fe-N coordination with a peak at ca. 1.51 Å and a secondary peak corresponding to Fe-Co coordination at high *R* value of ca. 2.25 Å (*62*). The Fe-Co coordination agrees well with the feature of simulated Fe K-edge spectra obtained by DFT calculations based on a model with N-coordinated Fe-Co atomic pairs in the framework of carbon. In contrast, the isolated dispersion of Fe or Co single atoms in catalysts can be demonstrated by the deficiency of a metal-metal path in their FT-EXAFS spectra. Different from M-N-C structures with isolated metal centers in porphyrin-like coordination, the metal-metal bond of dual-metal centers results in the deformation of local coordination and modified electronic structure. Both Fe and Co site in the Fe-Co dual-site catalyst can bind oxygen strongly and thus facilitate the sufficient activation of O_2, resulting in the facile cleavage of O—O bond and boosted OER catalytic activity.

In addition, the wavelet transform (WT)–EXAFS analysis can be used to provide a more straightforward demonstration of the metal-metal interactions among metal single atoms. For example, to determine the metal-metal interactions between adjacent atoms in a dual-atom W_1Mo_1-NG and Mo_2-NG catalysts, the Mo K-edge WT-EXAFS results were analyzed with those of references. As shown in Fig. 6A, the WT signal related to Mo-Mo bond in Mo foil is not detected in both W_1Mo_1-NG and Mo_2-NG, indicating the absence of Mo-containing nanoparticles. Compared to MoO_3, the two intensity maxima in W_1Mo_1-NG and Mo_2-NG at 3.9 and 9.3 $Å^{-1}$ can be respectively assigned to Mo-O and Mo-O-W/Mo paths. This provides strong and visualized evidence of the Mo-W/Mo interaction in the hetero/homonuclear C-SACs. In addition, compared with the fitting of FT-EXAFS that evaluates local coordination environment by separating the neighboring atoms according to their distances from the central atom, the WT-EXAFS offers to discriminate different atoms within one atomic shell by resolving the backscattering wave functions in energy space. This makes the WT-EXAFS more suitable for shells consisting of more than one type of atoms, e.g., the second shell of metal atoms supported on metal-based substrates. For example, in $Ir_{0.06}Co_{2.94}O_4$ catalyst with correlated Ir single atoms integrated in the lattice Co oxide spinel, the Ir centers exhibit a second-shell coordination derived from both Co and Ir. The WT-EXAFS result demonstrates a second-shell domain with dual local maxima, unambiguously identifying the coexistence of Ir-Co and Ir-Ir scatterings.

Fourier transform infrared spectroscopy

Some in situ spectroscopic techniques can be performed to detect the local structure of metal centers by evaluating their chemisorption behavior toward probe molecules. In situ diffuse reflectance infrared Fourier transform spectroscopy (DRIFTS) of CO chemisorption measurements represent an efficient technique for examining the local structure of metal centers, especially noble metals that show strong CO chemisorption. On one hand, the noble metal single atoms contrast with the corresponding noble metal nanoparticles as the latter exhibit bridge adsorption of CO with characteristic absorption

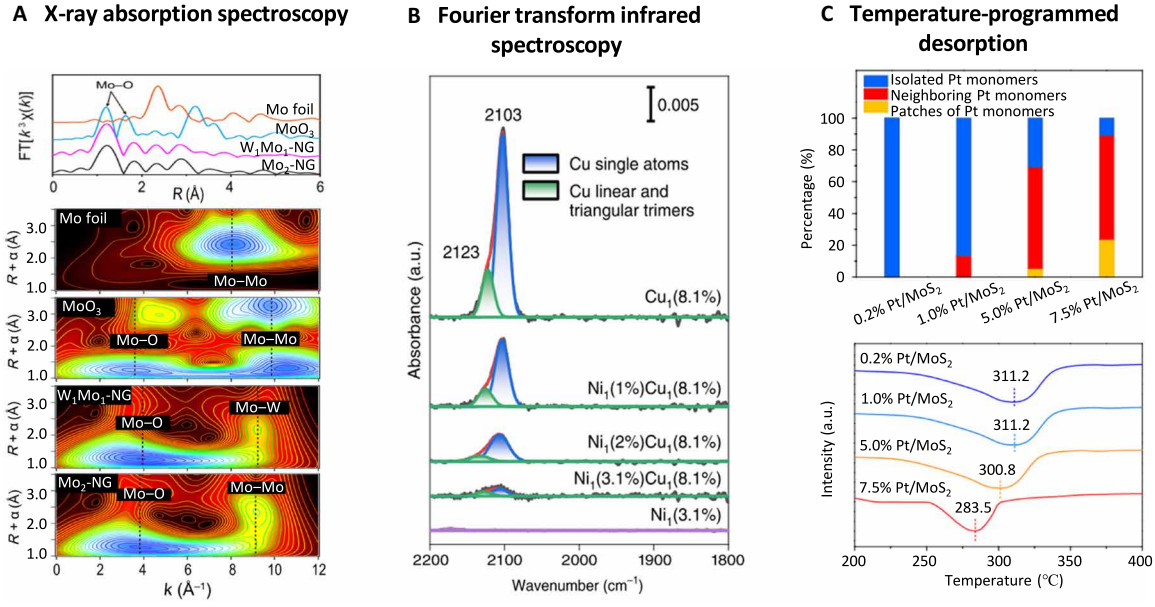

Fig. 6. The local coordination analysis of C-SACs with metal-metal interactions. (**A**) Mo K-edge FT-EXAFS and WT-EXAFS spectra of W_1Mo_1-NG and the references. Reproduced with permission from the American Association for the Advancement of Science (*76*). (**B**) CO-DRIFTS chemisorption spectra of correlated Ni-Cu catalysts. The CO chemisorption on Cu sites was weakened with the increase of Ni concentration, demonstrating the strong Ni-Cu interaction. Copied with permission from the Nature Publishing Group (*55*). (**C**) H_2-TPD profiles of atomically dispersed Pt/MoS_2 with different Pt loadings. Copied with permission from the Nature Publishing Group (*22*).

features at ~1850 cm^{-1}, whereas the single atoms show linear adsorption of CO at above 2000 cm^{-1} (*89*). On the other hand, as demonstrated by theoretical calculations and verified by experimental measurements, the correlated noble metal single atoms can be distinguished from isolated single atoms by different CO chemisorption peaks (*53*, *97*). In addition, the atomic interaction between correlated metal sites may affect the CO chemisorption behavior of target metal centers, making it an ideal measure to detect local environment by CO-DRIFTS. For instance, in a Ni_1Cu_2/g-C_3N_4 catalyst with one atomic Ni centers confined by two Cu grippers, the direct Cu-Ni interactions can be confirmed by in situ CO-DRIFTS chemisorption measurements in comparison with that of Ni_1/g-C_3N_4 and Cu_1/g-C_3N_4 with only one type of metal sites. As shown in Fig. 6B, Cu_1/g-C_3N_4 reveals evident CO chemisorption peaks at 2103 and 2123 cm^{-1} on isolated Cu^+ ions and trimers, respectively, while Ni_1/g-C_3N_4 shows negligible CO chemisorption. With the deposition of Ni atoms on Cu_1/g-C_3N_4, the intensity of CO peak gradually diminishes, strongly verifying the significantly decreased CO chemisorption on Cu sites due to direct Cu-Ni interactions.

Temperature-programmed desorption

In addition to DRIFTS, TPD measurements can be adopted to demonstrate the interaction among correlated single atoms by evaluating the adsorption/desorption behavior toward various gas molecules. For example, Li *et al.* (*22*) applied H_2-TPD to investigate the H_2 desorption behavior on Pt/MoS_2 catalysts with various Pt contents (Fig. 6C). The Pt/MoS_2 catalysts with mainly isolated Pt single atoms show similar H_2 desorption temperature at around 311.2°C, while with the increase of Pt content to form correlated Pt sites, the corresponding H_2 desorption temperature can be greatly lowered to 283.5°C. This result indicates the promoted dissociation of H_2 on the correlated Pt sites with synergistic interaction, which allows for manipulation of catalytic properties toward CO_2 hydrogenation. In addition, in a recent study of MnO_2-hosted adjacent Fe SAC, the O_2-TPD profile exhibited an additional characteristic peak at 192°C compared with that of pure MnO_2 (*48*). This suggests the emergence of new oxygen species formed on the correlated Fe sites, leading to a stronger O_2 activation and enhanced CO oxidation performance.

ELECTRONIC STRUCTURE INVESTIGATION

The variations in atomic structure and local coordination of correlated single metal atoms influence their electronic structure via orbital hybridization and charge transfer. At the same time, the incorporation of metal sites may cause notable modification of electronic structure of the substrate, resulting in changes in physicochemical properties of the hybrid materials (*98*). DFT calculations provide theoretical means for evaluating the electronic structure of C-SACs. On the basis of the rational structure modeling, the intrinsic properties of hybrid materials and their catalytic performance can be investigated from both thermodynamic and kinetic viewpoints.

Structural modeling

To intuitively analyze the electronic structures of correlated single atoms, the rational modeling of the hybrid structures is of great importance. For example, to investigate the electronic structure of short-range correlated Ir sites within the lattice of Co_3O_4, we constructed a series of Ir_4-$Co_{44}O_{64}$ models, where the interatomic distances among the four Ir sites were tuned to represent Ir clusters with diverse sizes (Fig. 7A) (*26*). When three Ir sites exhibit the nearest interatomic distances of $d_1 \approx d_2 \approx d_3$ (≈2.88 Å for this structure) with each other and the fourth Ir site show a much larger interatomic distance of d_4, the cluster size can be determined as 3 (atoms); when all Ir sites exhibit the interatomic distances larger than 2.88 Å with each other, they can be regarded as fully isolated single atoms; thus, the cluster size can be determined as 1 (atom). This definition is based on the premise that two single atoms distributed in the nearest interatomic distance can be deemed to be interactive with each other to form correlated sites. Another condition of this modeling is that the size of the supercell should be large enough to incorporate the Ir sites with designed interatomic distances. Therefore, based on the regulation above, the models of correlated Ir sites with 1 to 4 atom cluster size were created, respectively.

Structural thermostability

In SACs, theoretical calculations can be conducted to predict the possibility of integrating certain types of single atoms into the framework of the substrate by evaluating the thermodynamic stability of the hybrid system. Taking M′ substituted MO_x hybrid as an example, to achieve this, a ternary phase diagram including the atomic chemical potentials (μ_M, $\mu_{M'}$, and μ_O) of the component elements can be constructed to determine the formation energy of the possible competing phases in the system. When the equations corresponding to various competing phases (M′-MO_x hybrid material and various pure M′ oxides) are solved to obtain the varying ranges of atomic chemical potentials, the thermodynamic stability of target M′-MO_x hybrid phase can be determined. As shown in Fig. 7B, the existence of orange region in the diagram indicates that the equation of stable M′-MO_x phase can be solved under thermodynamic limitations to determine the ranges of μ_M, $\mu_{M'}$, and μ_O, suggesting the thermodynamically stable M′-MO_x structure with M′ atoms substituting the lattice sites in MO_x. In turn, the absence of phase corresponding to the hybrid structure in the ternary phase diagram would demonstrate that such a compound cannot exist against the competing phases.

Stability under reaction conditions

Currently, there is a lack of universally applicable theoretical investigations to evaluate the structural stability of catalysts under reaction conditions. For C-SACs, one can analyze the electronic structure and assess some parameters to explain and predict the catalytic properties. The valence band maximum (VBM) edge of metal sites, corresponding to the highest energy level occupied by electron states, can be adopted as an indicator to confirm the ability to lose electrons. As shown in Fig. 7C, upon incorporation of M′ single atoms, the hybrid M′-MO_x exhibits a down-shifting VBM of M-d band compared with the pure oxide in the density of states plot. This indicates that in the hybrid, it is less possible for the MO_x substrate to lose valence electrons, namely, to be (electro)chemically oxidized. This characteristics greatly enhances the structural stability of MO_x substrate under oxidative reaction conditions, well explaining the good catalytic stability of transition metal oxide-based catalysts in oxidation reactions, e.g., OER (*26*).

Thermodynamic energetics

C-SACs have been reported to exhibit unique catalytic properties, which can be attributed to the modulated adsorption behavior and

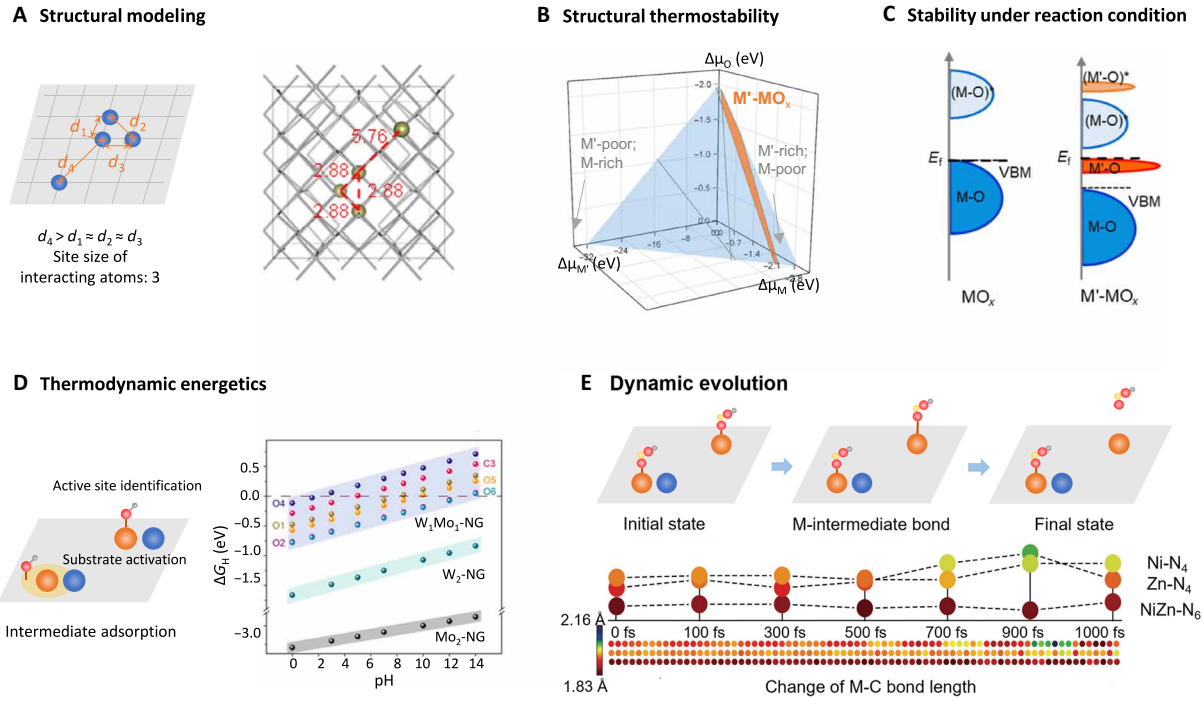

Fig. 7. The electronic structure investigation of C-SACs with metal-metal interactions. (**A**) Structure modeling of C-SACs. Copied with permission from the American Chemical Society (*26*). (**B**) A ternary phase diagram including the atomic chemical potentials (μ_M, $\mu_{M'}$, and μ_O) of the component elements. The structural thermostability of the hybrid material M′-MO$_x$ against competing phases can be determined. (**C**) The density of states of metal oxide substrate exhibits downshift of valance band maximum (VBM) upon metal single-atom incorporation. Copied with permission from the American Chemical Society (*26*). (**D**) Thermodynamic energetics evaluation on C-SACs. The ΔG_H of all the possible various sites were calculated to determine the active sites. Reproduced with permission from the American Association for the Advancement of Science (*76*). (**E**) Dynamic evolution study of C-SACs during reaction. Ab initio molecular dynamics (AIMD) calculations of the structure of the *COOH adsorption/desorption on NiZn-N$_6$, Ni-N$_4$, and Zn-N$_4$ catalysts with respect to the change in M-C bond length with time. Reproduced with permission from John Wiley and Sons (*93*).

energetics toward reaction intermediates. Extensive research efforts have been made to study the thermodynamic energetics, which can be used to investigate a series of reaction parameters, e.g., active sites (*68*), rate determining step (*99*), reaction pathway (*100*), etc. A major characteristic of C-SACs is the complicated atomic structure in comparison to the conventional isolated SACs, leading to more possibilities of the active sites during reactions. One can calculate and compare the Gibbs free energy (ΔG) for the possible models to determine the active sites in C-SACs and to evaluate the activity origin. For example, in an N-doped graphene-supported W-Mo heterodimer catalyst (W$_1$Mo$_1$-NG), a W-O-Mo-O-C configuration with O-coordinated W-Mo atoms in NG vacancies can be indicated by the combination of optimized DFT geometrical analysis and EXAFS fitting results (*76*). Correspondingly, nine possible active sites were suggested in W$_1$Mo$_1$-NG heterodimer. Taking the competing phases of homonuclear Mo$_2$-NG and W$_2$-NG systems into consideration, ΔG of H atom adsorption was calculated for all the possible active sites. As concluded in Fig. 7D, ΔG_H of active sites in heteronuclear W$_1$Mo$_1$-NG is much closer to the optimal condition than that in homonuclear systems throughout the whole pH range. In particular, the lattice O$_1$ site provides an optimal ΔG_H, suggesting that the W-Mo heterodimer activated the lattice O site to form a unique O-coordinated active ingredient for hydrogen evolution reaction (HER) under given pH condition.

Dynamic evolution

Chemical reactions are ingenious dynamic processes with many influence factors involved. For catalytic reactions promoted by C-SACs, the synergistic effect of correlated metal atoms plays a key role in facilitating the reaction processes. In general, electrochemical measurements (e.g., Tafel plots) and some in situ characterizations can be applied to investigate the contributions of these synergistic effects on the reaction kinetics (*101*). However, to explain this synergistic effect in-depth and intuitively, theoretical calculations and molecular dynamics simulations are required in term of the dynamic changes in the target structure. For instance, through calculating the activation energy (E_a) and exploring the carbon-metal (C-M) bond distances, the intrinsic synergistic effect of Ni-Zn paired-metal sites in NiZn-N$_6$ was analyzed (*93*). Specifically, the climbing image nudged elastic band (CI-NEB) result demonstrated a much lower E_a in the CO_2 hydrogenation reaction on the correlated Ni-Zn bimetal sites in comparison with that for the isolated metal single atoms. In addition, the ab initio molecular dynamics (AIMD) simulations show that the C-metal bond length between *COOH intermediate and the correlated NiZn-N$_6$ catalyst is relatively stable during the catalytic process, while those in the isolated SACs (Zn-N$_4$ and Ni-N$_4$) elongate rapidly (Fig. 7E). This finding confirmed the thermostability of the adsorbed *COOH intermediate on the correlated Ni-Zn sites. Therefore, the combination of CI-NEB and AIMD simulations has been used to demonstrate boosted reaction kinetics of CO_2RR on the correlated Ni-Zn bimetal sites.

SUMMARY AND OUTLOOK

In the past decade, a tremendous development in the structure design and fundamental electrocatalytic investigations on SACs has

been achieved, which resulted in the next-generation catalysts with maximum atomic utilization. However, the structure simplicity of SACs significantly restricts the substantial enhancement of their electrocatalytic performance. C-SACs can break such limitation by providing flexible structure with tunable atomic structure, local coordination, and electronic structure while maintaining the high atomic utilization. We propose here that the electronic structure modulation in C-SACs is dictated by the interaction between the central metal single atoms, which are closely associated with geometric structure of the correlated single atoms. So far, the investigation of the metal-metal interactions in C-SACs is still in its infancy stage. A few key problems are yet to be addressed to pave the way for future developments.

First, the precise control of atomic structure in C-SACs via general synthetic strategy remains to be a grant challenge. Common wet chemistry strategies feature easy implementation and low cost but are often difficult to obtain metal sites with precisely controlled local coordination and narrow size distribution. Although strategies such as ALD and mass-selected cluster deposition have been used to prepare small clusters supported on the surface of substrate or located in the lattice of substrate, the complicated synthetic procedure and the narrow choice of substrates greatly restrict their wide applicability. One promising methodology is to adopt self-assembly of metal precursors before deposition on an appropriate substrate.

Second, the comprehensive characterizations of C-SACs, especially the metal-metal interactions that exist in them, are still difficult to implement. Structural variables such as cluster size and local coordination configuration make the characterization of correlated single atoms more complicated than that of isolated single atoms in conventional SACs. In addition, the commonly used irregular carbon-based substrates and three-dimensional metal compound substrates both cause difficulty in unambiguous structure identification of C-SACs by microscopic techniques. On the other hand, because the concept of metal-metal interactions has not been brought up before, the detailed characterization of metal-metal interactions in C-SACs is limited.

Last but not the least, C-SACs represent a new metal geometry that bridges the conventional metal bulk crystals, nanoparticles, and isolated single atoms, yet the topological structure of correlated single atoms remains seldom studied. We propose here that the topological structure of correlated metal single atoms can be regulated by the choice of appropriate substrates and the careful integration of metal sites into the substrates. This strategy will greatly diversify the topological structure of metal single atoms and enable substantial modulation of electronic structure and catalytic properties of C-SACs.

Benefiting from great structural tunability facilitated by metal-metal interactions, C-SACs are promising candidates for next-generation highly efficient catalysts toward not only electrocatalytic reactions but also other critical heterogenous catalytic applications. In the current stage, a special emphasis should be on the research toward commercialization of these advanced materials.

REFERENCES AND NOTES

1. J. K. Nørskov, F. Studt, F. Abild-Pedersen, T. Bligaard, *Fundamental Concepts in Heterogeneous Catalysis* (John Wiley & Sons Inc., 2014).
2. G. C. Bond, in *Homogeneous and Heterogeneous Catalysis by Noble Metals* (Johnson, Matthey and Co. Ltd., 1974), vol. 70, pp. 25–34.
3. A. Wang, J. Li, T. Zhang, Heterogeneous single-atom catalysis. *Nat. Rev. Chem.* **2**, 65–81 (2018).
4. Z. W. Seh, J. Kibsgaard, C. F. Dickens, I. Chorkendorff, J. K. Nørskov, T. F. Jaramillo, Combining theory and experiment in electrocatalysis: Insights into materials design. *Science* **355**, eaad4998 (2017).
5. X.-F. Yang, A. Wang, B. Qiao, J. Li, J. Liu, T. Zhang, Single-atom catalysts: A new frontier in heterogeneous catalysis. *Acc. Chem. Res.* **46**, 1740–1748 (2013).
6. B. Qiao, A. Wang, X. Yang, L. F. Allard, Z. Jiang, Y. Cui, J. Liu, J. Li, T. Zhang, Single-atom catalysis of CO oxidation using Pt_1/FeO_x. *Nat. Chem.* **3**, 634–641 (2011).
7. Z. Geng, Y. Liu, X. Kong, P. Li, K. Li, Z. Liu, J. Du, M. Shu, R. Si, J. Zeng, Achieving a record-high yield rate of 120.9 ugNH3 mgcat.-1 h-1 for N_2 electrochemical reduction over Ru single-atom catalysts. *Adv. Mater.* **30**, 1803498 (2018).
8. D. Ji, L. Fan, L. Li, S. Peng, D. Yu, J. Song, S. Ramakrishna, S. Guo, Atomically transition metals on self-supported porous carbon flake arrays as binder-free air cathode for wearable zinc-air batteries. *Adv. Mater.* **31**, 1808267 (2019).
9. H. Jeong, D. Shin, B. S. Kim, J. Bae, S. Shin, C. Choe, J. W. Han, H. Lee, Controlling the oxidation state of Pt single atoms for maximizing catalytic activity. *Angew. Chem. Int. Ed.* **59**, 20691–20696 (2020).
10. J. Yin, J. Jin, M. Lu, B. Huang, H. Zhang, Y. Peng, P. Xi, C. H. Yan, Iridium single atoms coupling with oxygen vacancies boosts oxygen evolution reaction in acid media. *J. Am. Chem. Soc.* **142**, 18378–18386 (2020).
11. H. Zhang, S. Zuo, M. Qiu, S. Wang, Y. Zhang, J. Zhang, X. W. Lou, Direct probing of atomically dispersed Ru species over multi-edged TiO_2 for highly efficient photocatalytic hydrogen evolution. *Sci. Adv.* **6**, eabb9823 (2020).
12. R. Shen, W. Chen, Q. Peng, S. Lu, L. Zheng, X. Cao, Y. Wang, W. Zhu, J. Zhang, Z. Zhuang, C. Chen, D. Wang, Y. Li, High-concentration single atomic pt sites on hollow CuS_x for selective O_2 reduction to H_2O_2 in acid solution. *Chem* **5**, 2099–2110 (2019).
13. C. Gao, S. Chen, Y. Wang, J. Wang, X. Zheng, J. Zhu, L. Song, W. Zhang, Y. Xiong, Heterogeneous single-atom catalyst for visible-light-driven high-turnover CO_2 reduction: The role of electron transfer. *Adv. Mater.* **30**, 1704624 (2018).
14. J. Li, S. Sun, Intermetallic nanoparticles: Synthetic control and their enhanced electrocatalysis. *Acc. Chem. Res.* **52**, 2015–2025 (2019).
15. T. D. Spivey, A. Holewinski, Selective interactions between free-atom-liked-states in single-atom alloy catalysts and near-frontier molecular orbitals. *J. Am. Chem. Soc.* **143**, 11897–11902 (2021).
16. J. Yang, W. Li, D. Wang, Y. Li, Electronic metal-support interaction of single-atom catalysts and applications in electrocatalysis. *Adv. Mater.* **32**, 2003300 (2020).
17. C. T. Campbell, Electronic perturbations. *Nat. Chem.* **4**, 597–598 (2012).
18. Y. Ying, X. Luo, J. Qiao, H. Huang, "More is different:" Synergistic effect and structural engineering in double-atom catalysts. *Adv. Funct. Mater.* **31**, 2007423 (2021).
19. L. Liu, A. Corma, Metal catalysts for heterogeneous catalysis: From single atoms to nanoclusters and nanoparticles. *Chem. Rev.* **118**, 4981–5079 (2018).
20. C. Chu, D. Huang, S. Gupta, S. Weon, J. Niu, E. Stavitski, C. Muhich, J. H. Kim, Neighboring Pd single atoms surpass isolated single atoms for selective hydrodehalogenation catalysis. *Nat. Commun.* **12**, 5179 (2021).
21. Z. Jin, P. Li, Y. Meng, Z. Fang, D. Xiao, G. Yu, Understanding the inter-site distance effect in single-atom catalysts for oxygen electroreduction. *Nat. Catal.* **4**, 615–622 (2021).
22. H. Li, L. Wang, Y. Dai, Z. Pu, Z. Lao, Y. Chen, M. Wang, X. Zheng, J. Zhu, W. Zhang, R. Si, C. Ma, J. Zeng, Synergetic interaction between neighbouring platinum monomers in CO_2 hydrogenation. *Nat. Nanotechnol.* **13**, 411–417 (2018).
23. L. Jiao, J. Zhu, Y. Zhang, W. Yang, S. Zhou, A. Li, C. Xie, X. Zheng, W. Zhou, S. H. Yu, H. L. Jiang, Non-bonding interaction of neighboring Fe and Ni single-atom pairs on MOF-derived N-doped carbon for enhanced CO_2 electroreduction. *J. Am. Chem. Soc.* **143**, 19417–19424 (2021).
24. X. Zhao, F. Wang, X. P. Kong, R. Fang, Y. Li, Dual-metal hetero-single-atoms with different coordination for efficient synergistic catalysis. *J. Am. Chem. Soc.* **143**, 16068–16077 (2021).
25. B. Lu, Q. Liu, S. Chen, Electrocatalysis of single-atom sites: Impacts of atomic coordination. *ACS Catal.* **10**, 7584–7618 (2020).
26. J. Shan, C. Ye, S. Chen, T. Sun, Y. Jiao, L. Liu, C. Zhu, L. Song, Y. Han, M. Jaroniec, Y. Zhu, Y. Zheng, S. Z. Qiao, Short-range ordered iridium single atoms integrated into cobalt oxide spinel structure for highly efficient electrocatalytic water oxidation. *J. Am. Chem. Soc.* **143**, 5201–5211 (2021).
27. Z. Lu, B. Wang, Y. Hu, W. Liu, Y. Zhao, R. Yang, Z. Li, J. Luo, B. Chi, Z. Jiang, M. Li, S. Mu, S. Liao, J. Zhang, X. Sun, An isolated zinc-cobalt atomic pair for highly active and durable oxygen reduction. *Angew. Chem. Int. Ed.* **58**, 2622–2626 (2019).
28. Z. Zeng, L. Y. Gan, H. Bin Yang, X. Su, J. Gao, W. Liu, H. Matsumoto, J. Gong, J. Zhang, W. Cai, Z. Zhang, Y. Yan, B. Liu, P. Chen, Orbital coupling of hetero-diatomic nickel-iron site for bifunctional electrocatalysis of CO_2 reduction and oxygen evolution. *Nat. Commun.* **12**, 4088 (2021).
29. P. Zhou, X. Hou, Y. Chao, W. Yang, W. Zhang, Z. Mu, J. Lai, F. Lv, K. Yang, Y. Liu, J. Li, J. Ma, J. Luo, S. Guo, Synergetic interaction between neighboring platinum and ruthenium monomers boosts CO oxidation. *Chem. Sci.* **10**, 5898–5905 (2019).
30. X. Li, X. Yang, Y. Huang, T. Zhang, B. Liu, Supported noble-metal single atoms for heterogeneous catalysis. *Adv. Mater.* **31**, 1902031 (2019).
31. G. Pacchioni, Electronic interactions and charge transfers of metal atoms and clusters on oxide surfaces. *Phys. Chem. Chem. Phys.* **15**, 1737–1757 (2013).

32. C. M. Farley, C. Uyeda, Organic reactions enabled by catalytically active metal–metal bonds. *Trends Chem.* **1**, 497–509 (2019).
33. W. Qu, X. Liu, J. Chen, Y. Dong, X. Tang, Y. Chen, Single-atom catalysts reveal the dinuclear characteristic of active sites in NO selective reduction with NH3. *Nat. Commun.* **11**, 1532 (2020).
34. T. Imaoka, Y. Akanuma, N. Haruta, S. Tsuchiya, K. Ishihara, T. Okayasu, W. J. Chun, M. Takahashi, K. Yamamoto, Platinum clusters with precise numbers of atoms for preparative-scale catalysis. *Nat. Commun.* **8**, 688 (2017).
35. M. A. Hunter, J. M. T. A. Fischer, Q. Yuan, M. Hankel, D. J. Searles, Evaluating the catalytic efficiency of paired, single-atom catalysts for the oxygen reduction reaction. *ACS Catal.* **9**, 7660–7667 (2019).
36. L. Cheng, X. Yue, L. Wang, D. Zhang, P. Zhang, J. Fan, Q. Xiang, Dual-single-atom tailoring with bifunctional integration for high-performance CO_2 photoreduction. *Adv. Mater.* **33**, 2105135 (2021).
37. Z. Liu, F. Huang, M. Peng, Y. Chen, X. Cai, L. Wang, Z. Hu, X. Wen, N. Wang, D. Xiao, H. Jiang, H. Sun, H. Liu, D. Ma, Tuning the selectivity of catalytic nitriles hydrogenation by structure regulation in atomically dispersed Pd catalysts. *Nat. Commun.* **12**, 6194 (2021).
38. M. Peng, C. Dong, R. Gao, D. Xiao, H. Liu, D. Ma, Fully exposed cluster catalyst (FECC): Toward rich surface sites and full atom utilization efficiency. *ACS Cent. Sci.* **7**, 262–273 (2020).
39. T. He, A. R. P. Santiago, Y. Kong, M. A. Ahsan, R. Luque, A. du, H. Pan, Atomically dispersed heteronuclear dual-atom catalysts: A new rising star in atomic catalysis. *Small* **17**, e2106091 (2021).
40. I. G. Powers, C. Uyeda, Metal–metal bonds in catalysis. *ACS Catal.* **7**, 936–958 (2016).
41. T. He, A. R. Puente Santiago, A. Du, Atomically embedded asymmetrical dual-metal dimers on N-doped graphene for ultra-efficient nitrogen reduction reaction. *J. Catal.* **388**, 77–83 (2020).
42. J. Jiang, W. Ding, W. Li, Z. Wei, Freestanding single-atom-layer Pd-based catalysts: Oriented splitting of energy bands for unique stability and activity. *Chem* **6**, 431–447 (2020).
43. H. Cheng, X. Wu, M. Feng, X. Li, G. Lei, Z. Fan, D. Pan, F. Cui, G. He, Atomically dispersed Ni/Cu dual sites for boosting the CO2 reduction reaction. *ACS Catal.* **11**, 12673–12681 (2021).
44. S. Li, A. Guan, C. Yang, C. Peng, X. Lv, Y. Ji, Y. Quan, Q. Wang, L. Zhang, G. Zheng, Dual-atomic Cu sites for electrocatalytic CO reduction to C_{2+} products. *ACS Mater. Lett.* **3**, 1729–1737 (2021).
45. Y. Wang, B. J. Park, V. K. Paidi, R. Huang, Y. Lee, K. J. Noh, K. S. Lee, J. W. Han, Precisely constructing orbital coupling-modulated dual-atom fe pair sites for synergistic CO_2 electroreduction. *ACS Energy Lett.* **7**, 640–649 (2022).
46. Y. Ren, Y. Tang, L. Zhang, X. Liu, L. Li, S. Miao, D. Sheng Su, A. Wang, J. Li, T. Zhang, Unraveling the coordination structure-performance relationship in Pt_1/Fe_2O_3 single-atom catalyst. *Nat. Commun.* **10**, 4500 (2019).
47. Y. Pan, Y. Chen, K. Wu, Z. Chen, S. Liu, X. Cao, W. C. Cheong, T. Meng, J. Luo, L. Zheng, C. Liu, D. Wang, Q. Peng, J. Li, C. Chen, Regulating the coordination structure of single-atom Fe-N_xC_y catalytic sites for benzene oxidation. *Nat. Commun.* **10**, 4290 (2019).
48. H. Gu, X. Liu, X. Liu, C. Ling, K. Wei, G. Zhan, Y. Guo, L. Zhang, Adjacent single-atom irons boosting molecular oxygen activation on MnO_2. *Nat. Commun.* **12**, 5422 (2021).
49. X. Meng, C. Ma, L. Jiang, R. Si, X. Meng, Y. Tu, L. Yu, X. Bao, D. Deng, Distance synergy of MoS_2 -confined rhodium atoms for highly efficient hydrogen evolution. *Angew. Chem. Int. Ed.* **59**, 10502–10507 (2020).
50. X. Wang, S. Qiu, J. Feng, Y. Tong, F. Zhou, Q. Li, L. Song, S. Chen, K. H. Wu, P. Su, S. Ye, F. Hou, S. X. Dou, H. K. Liu, G. Q. (Max) Lu, C. Sun, J. Liu, J. Liang, Confined Fe–Cu clusters as sub-nanometer reactors for efficiently regulating the electrochemical nitrogen reduction reaction. *Adv. Mater.* **32**, 2004382 (2020).
51. Y. Zhao, W. J. Jiang, J. Zhang, E. C. Lovell, R. Amal, Z. Han, X. Lu, Anchoring sites engineering in single-atom catalysts for highly efficient electrochemical energy conversion reactions. *Adv. Mater.* **33**, 2102801 (2021).
52. Y. Hou, M. Qiu, M. G. Kim, P. Liu, G. Nam, T. Zhang, X. Zhuang, B. Yang, J. Cho, M. Chen, C. Yuan, L. Lei, X. Feng, Atomically dispersed nickel-nitrogen-sulfur species anchored on porous carbon nanosheets for efficient water oxidation. *Nat. Commun.* **10**, 1392 (2019).
53. H. Wang, J. X. Liu, L. F. Allard, S. Lee, J. Liu, H. Li, J. Wang, J. Wang, S. H. Oh, W. Li, M. Flytzani-Stephanopoulos, M. Shen, B. R. Goldsmith, M. Yang, Surpassing the single-atom catalytic activity limit through paired Pt-O-Pt ensemble built from isolated Pt1 atoms. *Nat. Commun.* **10**, 3808 (2019).
54. J. Wan, Z. Zhao, H. Shang, B. Peng, W. Chen, J. Pei, L. Zheng, J. Dong, R. Cao, R. Sarangi, Z. Jiang, D. Zhou, Z. Zhuang, J. Zhang, D. Wang, Y. Li, In situ phosphatizing of triphenylphosphine encapsulated within metal-organic frameworks to design atomic Co_1–P_1N_3 interfacial structure for promoting catalytic performance. *J. Am. Chem. Soc.* **142**, 8431–8439 (2020).
55. J. Gu, M. Jian, L. Huang, Z. Sun, A. Li, Y. Pan, J. Yang, W. Wen, W. Zhou, Y. Lin, H. J. Wang, X. Liu, L. Wang, X. Shi, X. Huang, L. Cao, S. Chen, X. Zheng, H. Pan, J. Zhu, S. Wei, W. X. Li, J. Lu, Synergizing metal-support interactions and spatial confinement boosts dynamics of atomic nickel for hydrogenations. *Nat. Nanotechnol.* **16**, 1141–1149 (2021).
56. X. Wan, X. Liu, Y. Li, R. Yu, L. Zheng, W. Yan, H. Wang, M. Xu, J. Shui, Fe–N–C electrocatalyst with dense active sites and efficient mass transport for high-performance proton exchange membrane fuel cells. *Nat. Catal.* **2**, 259–268 (2019).
57. F. Li, Y. Bu, G. F. Han, H. J. Noh, S. J. Kim, I. Ahmad, Y. Lu, P. Zhang, H. Y. Jeong, Z. Fu, Q. Zhong, J. B. Baek, Identifying the structure of Zn-N_2 active sites and structural activation. *Nat. Commun.* **10**, 2623 (2019).
58. F. Wu, C. Pan, C. T. He, Y. Han, W. Ma, H. Wei, W. Ji, W. Chen, J. Mao, P. Yu, D. Wang, L. Mao, Y. Li, Single-atom Co–N_4 electrocatalyst enabling four-electron oxygen reduction with enhanced hydrogen peroxide tolerance for selective sensing. *J. Am. Chem. Soc.* **142**, 16861–16867 (2020).
59. L. Ma, G. Zhu, D. Wang, H. Chen, Y. Lv, Y. Zhang, X. He, H. Pang, Emerging metal single atoms in electrocatalysts and batteries. *Adv. Funct. Mater.* **30**, 2003870 (2020).
60. T. Ding, X. Liu, Z. Tao, T. Liu, T. Chen, W. Zhang, X. Shen, D. Liu, S. Wang, B. Pang, D. Wu, L. Cao, L. Wang, T. Liu, Y. Li, H. Sheng, M. Zhu, T. Yao, Atomically precise dinuclear site active toward electrocatalytic CO_2 reduction. *J. Am. Chem. Soc.* **143**, 11317–11324 (2021).
61. X. Zeng, J. Shui, X. Liu, Q. Liu, Y. Li, J. Shang, L. Zheng, R. Yu, Single-atom to single-atom grafting of Pt_1 onto Fe–N_4Center: Pt_1@Fe-N-C multifunctional electrocatalyst with significantly enhanced properties. *Adv. Energy Mater.* **8**, 1701345 (2018).
62. J. Wang, Z. Huang, W. Liu, C. Chang, H. Tang, Z. Li, W. Chen, C. Jia, T. Yao, S. Wei, Y. Wu, Y. Li, Design of N-coordinated dual-metal sites: A stable and active Pt-free catalyst for acidic oxygen reduction reaction. *J. Am. Chem. Soc.* **139**, 17281–17284 (2017).
63. L. Zhang, R. Si, H. Liu, N. Chen, Q. Wang, K. Adair, Z. Wang, J. Chen, Z. Song, J. Li, M. N. Banis, R. Li, T. K. Sham, M. Gu, L. M. Liu, G. A. Botton, X. Sun, Atomic layer deposited Pt-Ru dual-metal dimers and identifying their active sites for hydrogen evolution reaction. *Nat. Commun.* **10**, 4936 (2019).
64. D. Liu, B. Wang, H. Li, S. Huang, M. Liu, J. Wang, Q. Wang, J. Zhang, Y. Zhao, Distinguished Zn,Co-N_x-C-S_y active sites confined in dentric carbon for highly efficient oxygen reduction reaction and flexible Zn-air batteries. *Nano Energy* **58**, 277–283 (2019).
65. C. Yan, H. Li, Y. Ye, H. Wu, F. Cai, R. Si, J. Xiao, S. Miao, S. Xie, F. Yang, Y. Li, G. Wang, X. Bao, Coordinatively unsaturated nickel–nitrogen sites towards selective and high-rate CO2 electroreduction. *Energy Environ. Sci.* **11**, 1204–1210 (2018).
66. Y. Zhang, L. Guo, L. Tao, Y. Lu, S. Wang, Defect-based single-atom electrocatalysts. *Small Methods* **3**, 1800406 (2018).
67. X. Zhang, J. Guo, P. Guan, C. Liu, H. Huang, F. Xue, X. Dong, S. J. Pennycook, M. F. Chisholm, Catalytically active single-atom niobium in graphitic layers. *Nat. Commun.* **4**, 1924 (2013).
68. W. Chen, W. Gao, P. Tu, T. Robert, Y. Ma, H. Shan, X. Gu, W. Shang, P. Tao, C. Song, T. Deng, H. Zhu, X. Pan, H. Yang, J. Wu, Neighboring Pt atom sites in an ultrathin FePt nanosheet for the efficient and highly CO-tolerant oxygen reduction reaction. *Nano Lett.* **18**, 5905–5912 (2018).
69. C.-L. Yang, L.-N. Wang, P. Yin, J. Liu, M.-X. Chen, Q.-Q. Yan, Z.-S. Wang, S.-L. Xu, S.-Q. Chu, C. Cui, H. Ju, J. Zhu, Y. Lin, J. Shui, H.-W. Liang, Sulfur-anchoring synthesis of platinum intermetallic nanoparticle catalysts for fuel cells. *Science* **374**, 459–464 (2021).
70. Z. Jakub, J. Hulva, M. Meier, R. Bliem, F. Kraushofer, M. Setvin, M. Schmid, U. Diebold, C. Franchini, G. S. Parkinson, Local structure and coordination define adsorption in a model Ir_1/Fe_3O_4 single-atom catalyst. *Angew. Chem. Int. Ed.* **58**, 13961–13968 (2019).
71. Q. Wang, X. Huang, Z. L. Zhao, M. Wang, B. Xiang, J. Li, Z. Feng, H. Xu, M. Gu, Ultrahigh-loading of Ir single atoms on NiO matrix to dramatically enhance oxygen evolution reaction. *J. Am. Chem. Soc.* **142**, 7425–7433 (2020).
72. X. Zhang, M. Zhang, Y. Deng, M. Xu, L. Artiglia, W. Wen, R. Gao, B. Chen, S. Yao, X. Zhang, M. Peng, J. Yan, A. Li, Z. Jiang, X. Gao, S. Cao, C. Yang, A. J. Kropf, J. Shi, J. Xie, M. Bi, J. A. van Bokhoven, Y.-W. Li, X. Wen, M. Flytzani-Stephanopoulos, C. Shi, W. Zhou, D. Ma, A stable low-temperature H_2-production catalyst by crowding Pt on α-MoC. *Nature* **589**, 396–401 (2021).
73. K. Jiang, M. Luo, M. Peng, Y. Yu, Y. R. Lu, T. S. Chan, P. Liu, F. M. F. de Groot, Y. Tan, Dynamic active-site generation of atomic iridium stabilized on nanoporous metal phosphides for water oxidation. *Nat. Commun.* **11**, 2701 (2020).
74. X. Liang, L. Shi, Y. Liu, H. Chen, R. Si, W. Yan, Q. Zhang, G.-D. Li, L. Yang, X. Zou, Activating inert, nonprecious perovskites with iridium dopants for efficient oxygen evolution reaction under acidic conditions. *Angew. Chem. Int. Ed.* **58**, 7631–7635 (2019).
75. X. Han, X. Ling, D. Yu, D. Xie, L. Li, S. Peng, C. Zhong, N. Zhao, Y. Deng, W. Hu, Atomically dispersed binary Co-Ni sites in nitrogen-doped hollow carbon nanocubes for reversible oxygen reduction and evolution. *Adv. Mater.* **31**, 1905622 (2019).
76. Y. Yang, Y. Qian, H. Li, Z. Zhang, Y. Mu, D. Do, B. Zhou, J. Dong, W. Yan, Y. Qin, L. Fang, R. Feng, J. Zhou, P. Zhang, J. Dong, G. Yu, Y. Liu, X. Zhang, X. Fan, O-coordinated W-Mo dual-atom catalyst for pH-universal electrocatalytic hydrogen evolution. *Sci. Adv.* **6**, eaba6586 (2020).

77. Y. Qiu, J. Zhang, J. Jin, J. Sun, H. Tang, Q. Chen, Z. Zhang, W. Sun, G. Meng, Q. Xu, Y. Zhu, A. Han, L. Gu, D. Wang, Y. Li, Construction of Pd-Zn dual sites to enhance the performance for ethanol electro-oxidation reaction. *Nat. Commun.* **12**, 5273 (2021).
78. N. E. Richey, C. de Paula, S. F. Bent, Understanding chemical and physical mechanisms in atomic layer deposition. *J. Chem. Phys.* **152**, 040902 (2020).
79. H. Yan, Y. Lin, H. Wu, W. Zhang, Z. Sun, H. Cheng, W. Liu, C. Wang, J. Li, X. Huang, T. Yao, J. Yang, S. Wei, J. Lu, Bottom-up precise synthesis of stable platinum dimers on graphene. *Nat. Commun.* **8**, 1070 (2017).
80. L. Bai, C. S. Hsu, D. T. L. Alexander, H. M. Chen, X. Hu, A cobalt-iron double-atom catalyst for the oxygen evolution reaction. *J. Am. Chem. Soc.* **141**, 14190–14199 (2019).
81. L. Bai, C.-S. Hsu, D. T. L. Alexander, H. M. Chen, X. Hu, Double-atom catalysts as a molecular platform for heterogeneous oxygen evolution electrocatalysis. *Nat. Energy* **6**, 1054–1066 (2021).
82. E. Vorobyeva, E. Fako, Z. Chen, S. M. Collins, D. Johnstone, P. A. Midgley, R. Hauert, O. V. Safonova, G. Vilé, N. López, S. Mitchell, J. Pérez-Ramírez, Atom-by-atom resolution of structure-function relations over low-nuclearity metal catalysts. *Angew. Chem. Int. Ed.* **58**, 8724–8729 (2019).
83. C. Dong, Y. Li, D. Cheng, M. Zhang, J. Liu, Y. G. Wang, D. Xiao, D. Ma, Supported metal clusters: Fabrication and application in heterogeneous catalysis. *ACS Catal.* **10**, 11011–11045 (2020).
84. R. Gao, J. Wang, Z. F. Huang, R. Zhang, W. Wang, L. Pan, J. Zhang, W. Zhu, X. Zhang, C. Shi, J. Lim, J. J. Zou, Pt/Fe_2O_3 with Pt–Fe pair sites as a catalyst for oxygen reduction with ultralow Pt loading. *Nat. Energy* **6**, 614–623 (2021).
85. C. Lin, J. L. Li, X. Li, S. Yang, W. Luo, Y. Zhang, S. H. Kim, D. H. Kim, S. S. Shinde, Y. F. Li, Z. P. Liu, Z. Jiang, J. H. Lee, In-situ reconstructed Ru atom array on α-MnO_2 with enhanced performance for acidic water oxidation. *Nat. Catal.* **4**, 1012–1023 (2021).
86. X. Hai, S. Xi, S. Mitchell, K. Harrath, H. Xu, D. F. Akl, D. Kong, J. Li, Z. Li, T. Sun, H. Yang, Y. Cui, C. Su, X. Zhao, J. Li, J. Pérez-Ramírez, J. Lu, Scalable two-step annealing method for preparing ultra-high-density single-atom catalyst libraries. *Nat. Nanotechnol.* **17**, 174–181 (2022).
87. M. Weyland, P. A. Midgley, J. M. Thomas, Electron tomography of nanoparticle catalysts on porous supports: A new technique based on Rutherford scattering. *J. Phys. Chem. B* **105**, 7882–7886 (2001).
88. N. Cheng, L. Zhang, K. Doyle-Davis, X. Sun, Single-atom catalysts: From design to application. *Electrochem. Energy Rev.* **2**, 539–573 (2019).
89. Y. Zhao, K. R. Yang, Z. Wang, X. Yan, S. Cao, Y. Ye, Q. Dong, X. Zhang, J. E. Thorne, L. Jin, K. L. Materna, A. Trimpalis, H. Bai, S. C. Fakra, X. Zhong, P. Wang, X. Pan, J. Guo, M. Flytzani-Stephanopoulos, G. W. Brudvig, V. S. Batista, D. Wang, Stable iridium dinuclear heterogeneous catalysts supported on metal-oxide substrate for solar water oxidation. *Proc. Natl. Acad. Sci. U.S.A.* **115**, 2902–2907 (2018).
90. C. Coll, L. López-Conesa, J. M. Rebled, C. Magén, F. Sánchez, J. Fontcuberta, S. Estradé, F. Peiró, Simulation of STEM-HAADF image contrast of Ruddlesden-Popper faulted $LaNiO_3$ thin films. *J. Phys. Chem. C* **121**, 9300–9304 (2017).
91. K. Qi, X. Cui, L. Gu, S. Yu, X. Fan, M. Luo, S. Xu, N. Li, L. Zheng, Q. Zhang, J. Ma, Y. Gong, F. Lv, K. Wang, H. Huang, W. Zhang, S. Guo, W. Zheng, P. Liu, Single-atom cobalt array bound to distorted 1T MoS_2 with ensemble effect for hydrogen evolution catalysis. *Nat. Commun.* **10**, 5231 (2019).
92. J. Zhang, Y. Zhao, X. Guo, C. Chen, C. L. Dong, R. S. Liu, C. P. Han, Y. Li, Y. Gogotsi, G. Wang, Single platinum atoms immobilized on an MXene as an efficient catalyst for the hydrogen evolution reaction. *Nat. Catal.* **1**, 985–992 (2018).
93. Y. Li, B. Wei, M. Zhu, J. Chen, Q. Jiang, B. Yang, Y. Hou, L. Lei, Z. Li, R. Zhang, Y. Lu, Synergistic effect of atomically dispersed Ni-Zn pair sites for enhanced CO_2 electroreduction. *Adv. Mater.* **33**, 2102212 (2021).
94. J. B. Souza Junior, G. R. Schleder, J. Bettini, I. C. Nogueira, A. Fazzio, E. R. Leite, Pair distribution function obtained from electron diffraction: An advanced real-space structural characterization tool. *Matter* **4**, 441–460 (2021).
95. E. A. Derevyannikova, T. Y. Kardash, A. I. Stadnichenko, O. A. Stonkus, E. M. Slavinskaya, V. A. Svetlichnyi, A. I. Boronin, Structural insight into strong Pt–CeO2 interaction: From single Pt Atoms to PtO_x clusters. *J. Phys. Chem. C* **123**, 1320–1334 (2018).
96. W. Ren, X. Tan, W. Yang, C. Jia, S. Xu, K. Wang, S. C. Smith, C. Zhao, Isolated diatomic Ni-Fe metal-nitrogen sites for synergistic electroreduction of CO2. *Angew. Chem. Int. Ed.* **58**, 6972–6976 (2019).
97. H. Jeong, G. Lee, B. S. Kim, J. Bae, J. W. Han, H. Lee, Fully dispersed Rh ensemble catalyst to enhance low-temperature activity. *J. Am. Chem. Soc.* **140**, 9558–9565 (2018).
98. Z.-H. Xue, D. Luan, H. Zhang, X. W. Lou, Single-atom catalysts for photocatalytic energy conversion. *Joule* **6**, 92–133 (2022).
99. X. Wang, Y. Li, Y. Wang, H. Zhang, Z. Jin, X. Yang, Z. Shi, L. Liang, Z. Wu, Z. Jiang, W. Zhang, C. Liu, W. Xing, J. Ge, Proton exchange membrane fuel cells powered with both CO and H_2. *Proc. Natl. Acad. Sci. U.S.A.* **118**, e2107332118 (2021).
100. M. Liu, N. Li, S. Cao, X. Wang, X. Lu, L. Kong, Y. Xu, X.-H. Bu, A "pre-constrained metal twins" strategy to prepare efficient dual-metal-atom catalysts for cooperative oxygen electrocatalysis. *Adv. Mater.* **34**, e2107421 (2022).
101. S. Zuo, Z. P. Wu, H. Zhang, X. W. Lou, Operando monitoring and deciphering the structural evolution in oxygen evolution electrocatalysis. *Adv. Energy Mater.* **12**, 2103383 (2022).

Acknowledgments

Funding: Y.Z. and S.-Z.Q. acknowledge financial support from the Australian Research Council (FL170100154, FT200100062, and DP190103472). **Author contributions:** J.S., Y.Z., and S.-Z.Q. conceived the topic of the Review. All authors contributed to discussions of the content. S.-Z.Q. and M.J. corrected and reviewed the article before submission. **Competing interests:** The authors declare that they have no competing interests. **Data and materials availability:** All data needed to evaluate the conclusions in the paper are present in the paper and/or the Supplementary Materials.

Submitted 12 January 2022
Accepted 16 March 2022
Published 29 April 2022
10.1126/sciadv.abo0762